Morphological and Electromechanical Studies of Fibers Coated with Electrically Conductive Polymer

P. Xue, X. M. Tao[1]

Institute of Textiles and Clothing, Hong Kong Polytechnic University, Kowloon, Hong Kong

Received 18 October 2004; accepted 4 February 2005
DOI 10.1002/app.22318
Published online in Wiley InterScience (www.interscience.wiley.com).

ABSTRACT: Electrically conductive fibers have been prepared by polymerization of pyrrole on surfaces of commercial polymer fibers. Thickness and morphology of the conducting thin film on the surface of the fibers were examined by scanning probe microscopy, indicating a strong dependence of the substrate's nature, in addition to the processing conditions. Electromechanical property was investigated by an electromechanical testing system, showing that a smooth and uniform coating and the matched mechanical properties will lead to a satisfied performance of conductive fiber sensors. The difference in the behavior of two types of composite fibers was investigated by scanning electron microscopy *in situ* observations. © 2005 Wiley Periodicals, Inc. J Appl Polym Sci 98: 1844–1854, 2005

Key words: polypyrroles; coatings; fibers; morphology; structure–property relations

INTRODUCTION

Intelligent materials and structures include three basic components, i.e., sensors, actuators, and controlling units.[1] Sensors, which provide nerve system to detect signals, are essential elements and become increasingly important. Micro- or submicrosized lightweight flexible fiber sensors are capable of measuring temperature, strain/stress, gas, biological species, and smell. Integrating these flexible sensors and their network into textiles will provide the possibility of *in situ* measurement in applications related to virtual reality, teleoperation, ergonomics, and rehabilitation engineering.

Many types of fiber sensors have been developed in the past decade, including fiber optic, piezoelectric, and electrically conducting sensors. Electrically conducting sensors, due to their relative simplicity in measurement, cost-effectiveness, and durablity, are receiving more attention. Electrically conductive fibers can be intrinsically conductive or become conductive by coating or blending or integrating with electrically conductive materials. Carbon fibers represent a class of intrinsically conducting fibers and have been used for sensing strain under tension[2,3] and bending loading[4] and to assess the damage in composites and monitor the damage in real time.[5,6] However, most of the carbon fibers possess a modulus in the order of 200 GPa or more, while most textile fibers have a modulus in the magnitude of several GPa. An introduction of the rigid carbon fibers into a textile structure may alter the strain field significantly. In addition, the measurement range of carbon-fiber-based sensors is limited to a small strain, while most fibers have an extensibility of over 10%. Therefore, it is important to explore new types of electrically conductive fibers to serve in these applications.

Conducting polymers, such as polyacetylene, polypyrrole, polythiophene, and polyaniline, offer an interesting alternative. As chemically or electrochemically doped liner π-conjugated polymers, they possess conductive property similar to that of metal.[7] Among these conductive polymers, polypyrrole (PPy) is regarded as one of the most promising intrinsically conducting polymers due to its relatively high electrical conductivity, good environmental stability under ambient conditions, and low toxicity.[8,9]

However, as a conjugated conducting polymer, PPy exhibits poor processability and lacks essential mechanical properties, which have limited its practical applications. Efforts to overcome these drawbacks have been made. Mechanically blending PPy powder with some polymers[10,11] is one of the approaches; nevertheless, the conductivity of the blends decreases substantially owing to aging during processing at elevated temperatures.[12] Furthermore, a rather high percentage (usually above 40 wt %) of PPy in the blends, to exceed the percolation threshold of conductivity, is required to produce com-

Correspondence to: X. Tao (tctaoxm@inet.polyu.edu.hk).
Contract grant sponsor: Innovation and Technology Commission of the Hong Kong SAR Government ; contract grant number: ITF project ITS/71/02; Contract grant sponsor: Hong Kong Research Grants Council; contract grant number: PolyU5160/02E.

posites with high conductivity. The high percentage of filler generally causes a dramatic deterioration of mechanical properties, such as deformability and toughness. Even a 10.6 wt % PPy filler could cause a 65% reduction in the elongation at break.[13] By imbibing pyrrole in Nylon 66 film followed by immersion in $FeCl_3$, the elongation at break of the N66/PPy composite film decreased drastically from 350% for N66 to 60% for N66/PPy.[14] To take the advantages of mechanical properties, processability, and cost of conventional polymers, it is necessary to keep the PPy concentration in the composites at a minimum. Another route to overcome the deficiency mentioned above is by coating conducting polymer to a flexible textile substrate, which is relative stable and can be easily handled.[15,16] Thus, PPy-based composites may overcome the deficiency of PPy's mechanical property without adversely affecting the excellent physical properties of the textile substrate such as mechanical strength and flexibility. The resulting products combine the advantages of a textile substrate with electrical properties similar to that of metals or semiconductors.

Despite the promising performance, however, understanding the electromechanical behavior of the PPy-coated conductive composites and controlling electrical conductivity by selecting the substrate, coating thickness, etc., are still in great and immediate demand. In our previous paper,[17] we reported the sensing behavior of PPy-coated polymer fibers. Their electromechanical behavior under tensile load was experimentally studied. In the present study, we will focus on morphology, conductivity, and mechanical properties of PPy-coated conductive fibers/yarn, and investigate in multiscale the mechanisms by which electrically conductive fibers perform by means of scanning probe microscopy (SPM), scanning electron microscopy (SEM), and an electromechanical testing system.

EXPERIMENTAL DETAILS

Materials and the preparation of samples

Considering the potential applications in intelligent textiles, two material systems were examined in the present study: polycaprolactam (PA6) fibers coated with PPy and polyurethane (PU) fibers (Lycra) coated with PPy. The commercial multifilaments of PA6 were supplied by Dupont, and PU yarn was supplied by Sunikorn Knitters (HK). Pyrrole (99%) and ferric chloride hexahydrate ($FeCl_3{\cdot}6H_2O$) were purchased from Sigma–Aldrich Chemical. All chemicals in the highest available grades were used as received. The linear density of the PA6 yarn is 702 denier/68F and that of PU yarn is 40 denier/5F.

PPy-coated fibers were obtained by chemical vapor deposition method. The fibers to be coated were fixed parallel on a support frame at some intervals and soaked in a 50 g/L $FeCl_3$ solution (used as the oxidizing agent) for 10 min. They were then taken out and the residual oxidizing solution on the fiber surface was removed by a filter paper. The fibers soaked with oxidizing agent were transferred to a glass desiccator in which a beaker containing l0 mL pyrrole monomer was placed. The desiccator with the fibers and pyrrole was first vacuum-suctioned and then opened to a nitrogen gas atmosphere at room temperature for 24 h. After the vapor deposition process, the PPy-coated fibers were taken out and washed in deionized water for 10 min. They were then put in a desiccator for drying before being measured. Samples of PPy-coated PA6 fibers and PPy-coated PU fibers were both prepared under the same procedure and conditions. As the PPy started to grow on the fibers with a polymerization in being exposed under pyrrole vapor, the initial white color of PA6 and PU fibers gradually became dark, and finally the color turned to black. This evolution depends on the concentration of $FeCl_3{\cdot}6H_2O$ aqueous solution, polymerization time, and temperature.

The samples for SPM examination on the cross-section were embedded in epoxy and cured. The sections for SPM observation were sliced from the top of a trimmed block using a Cryo Microtome under low temperature with liquid nitrogen. A silver paste was used to adhere the samples onto a conducting stage when doing AFM observation with a current measurement.

Characterization

SPM

Multimode measurements were carried out by a scanning probe microscope system (SPI4000/SPA300HV from Seiko Instruments) under ambient conditions. Standard silicon nitride tips were used. SPM images were obtained from cross-sections and the surface of a composite fiber, respectively. The thickness of the coating layer can be measured by the SPI4000 system. Dynamic force microscope (DFM) mode was applied to obtain the topographical images. AFM with current measurement mode was used to demonstrate the electrical conductivity of the PPy coating layer. Before scanning, AFM can be calibrated in the vertical direction by a grid sample with a fixed depth.

In situ SEM observation

A scanning electron microscope (Lecia Steroscan 440) integrating a material tester system was used to investigate the mechanisms that governed the eletromechanical behavior of the PPy-coated electrically conductive fibers. This system enables us simultaneously to observe in microscale the changes that occurred on the surface of the specimen and to record the load and displacement of

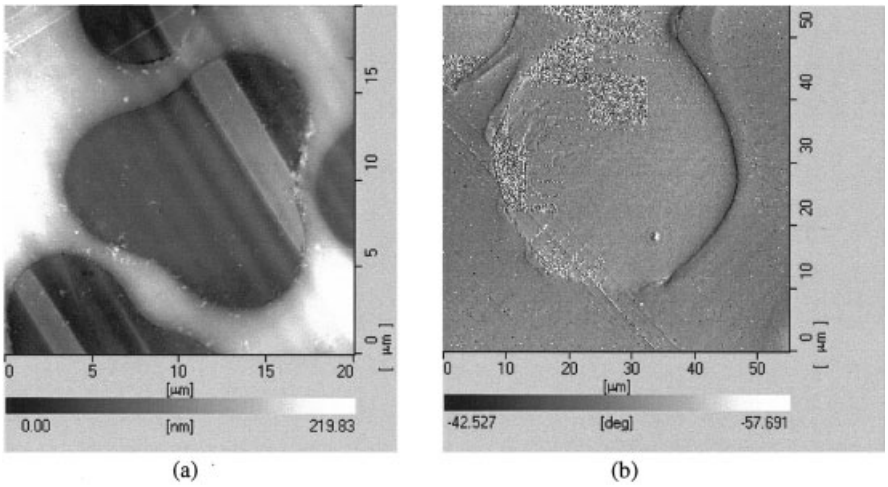

Figure 1 Topographical images of (a) PPy-coated PA6 fiber and (b) PPy-coated PU fiber.

the specimen during the tensile process. A single piece of yarn was attached on a sample holder with a gauge length of 10 mm, and then it was elongated at a constant loading speed of 2 mm/min. The microphotographs were obtained at an accelerating voltage of 5 kV for PPy-coated PU fibers and at higher accelerating voltage of 20 kV for PPy-coated PA6 fibers.

Measurement of electromechanical performance

The electrical resistance of the PPy-coated fibers was measured by the four-probe method with a Keithley 2010 Multimeter while the fibers were extended. The electrical contacts were made by using copper foils. The load and deformation were obtained and recorded using an Instron mechanical testing system. A single piece of yarn was attached to a paper frame before testing. The crosshead speed was 5 mm/min and the gauge length of each specimen was 50 mm. At least five specimens from each sample were tested and the average value was taken and standard deviations were calculated. All electromechanical tests were carried out at 20 °C and 65% RH.

EXPERIMENTAL RESULTS AND DISCUSSION

Geometry of the fibers and coating layer

The SPM topography images viewed on the cross-sections of PPy-coated PA6 fibers and PU fibers under DFM mode are shown in Figure 1. The oblique lines on the images are scratches during sample preparation. In Figure 1(a), the substrate fiber is shown in the darker region and the polymer used to embed the sample is in the lighter region; and in Figure 1(b) the substrate fiber is shown in the central region and the polymer used to embed the sample is in the side region. The electrically conductive layer exists between the two materials. These images show that the cross-sectional geometry of PA6 fiber is trilobal with height about 13 μm. The cross-sectional geometry of PU fiber is almost a circle with diameter about 40 μm. The variation in the cross-sectional geometry will affect moisture transport properties due to capillary action; however, little effect is expected on conductivity.

Figure 2(a) shows the phase image of PPy-coated PA6 fibers on the cross-section, indicating the coating layer between the substrate fiber and the polymer used to embed the sample. In Figure 2(b,c), the insulating region is shown in the darker region and the electrically conductive region in the lighter region. PPy displayed a continuous pathway of conductive domain with 200- to 300-nm in thickness on PA6 fiber base. In comparison, as shown in Figure 3, on the PU fiber base it could only identify a thinner and discontinuous electrically conductive domain with maximum thickness about 50 nm. The samples of PPy-coated PA6 fibers and PPy-coated PU fibers were both prepared under the same chemical deposition procedure and conditions, and therefore coating PPy on PA6 fiber base would lead to a better quality than that on PU fiber base. These views also account for the results, which will be given later, showing that the PPy-coated PA6 fibers macroscopically displayed much higher electrical conductivity than PPy-coated PU fibers.

Morphology of PPy coating layer

The morphological view of PPy coating on two kinds of fiber bases was examined by the SPM using the tapping mode. Figure 4(a) and 4(b) gives the phase images of PA6 fiber and PU fiber, respectively. Figure 4(c–f) shows the topographical views from different viewpoints. The morphology of the PPy coating films is highly dependent on the substrate.

During the surface topography imaging by SPM, one can measure the deflection of the cantilever asso-

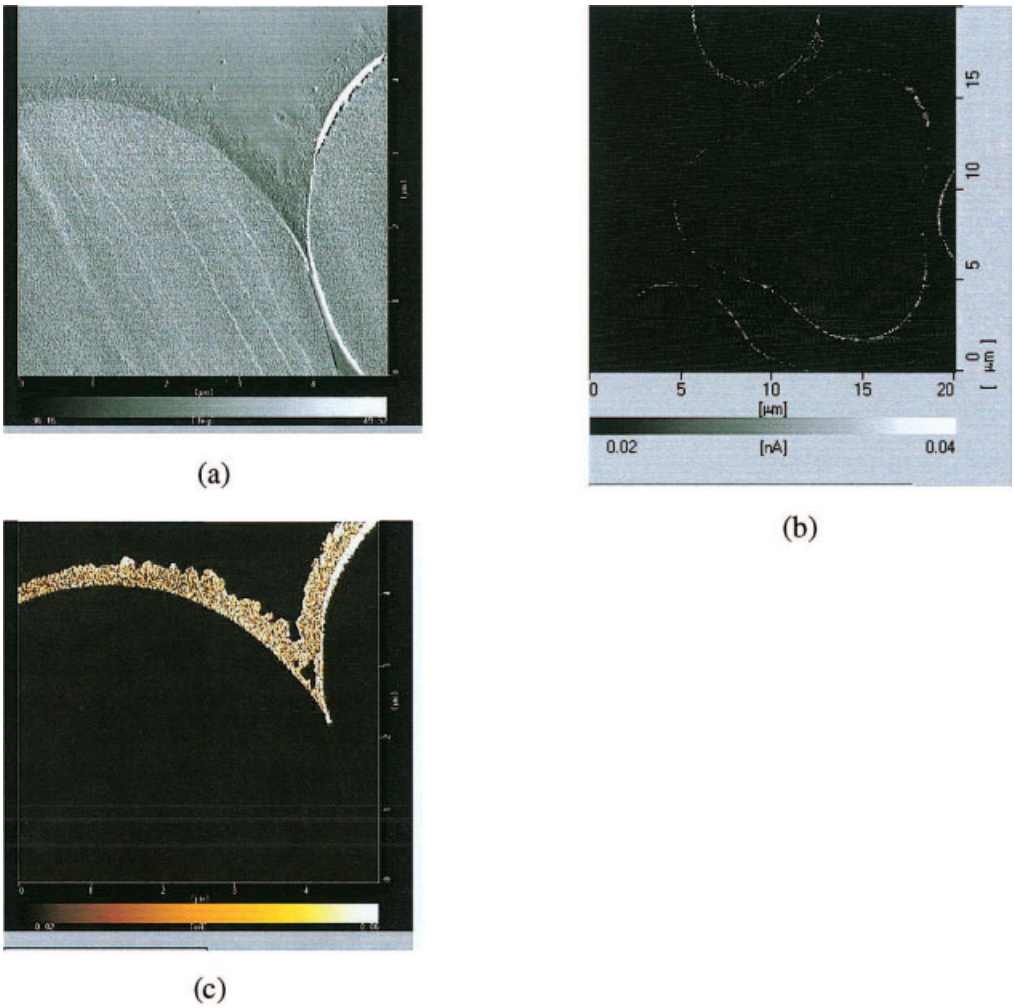

Figure 2 (a) Phase image of PPy-coated PA6 fiber; (b) a cross-sectional image by AFM with current measurement. The bias voltage applied is 2.5 V. (c) Enlarged image showing the conductive layer. The bias voltage applied is 1 V. [Color figure can be viewed in the online issue, which is available at www.interscience.wiley.com.]

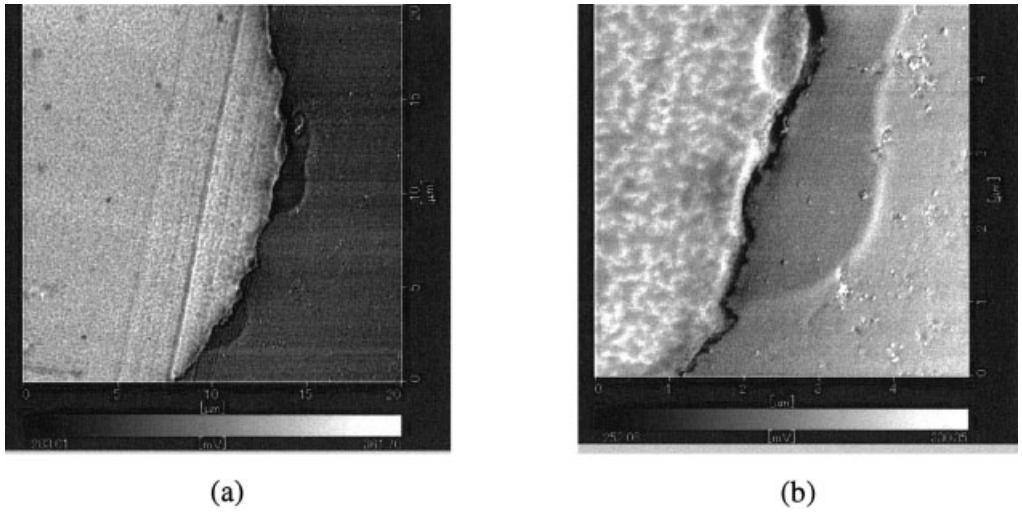

Figure 3 SPM images of the PPy-coated PU fiber. The observed area is (a) 20 × 20 μm and (b) 5 × 5 μm.

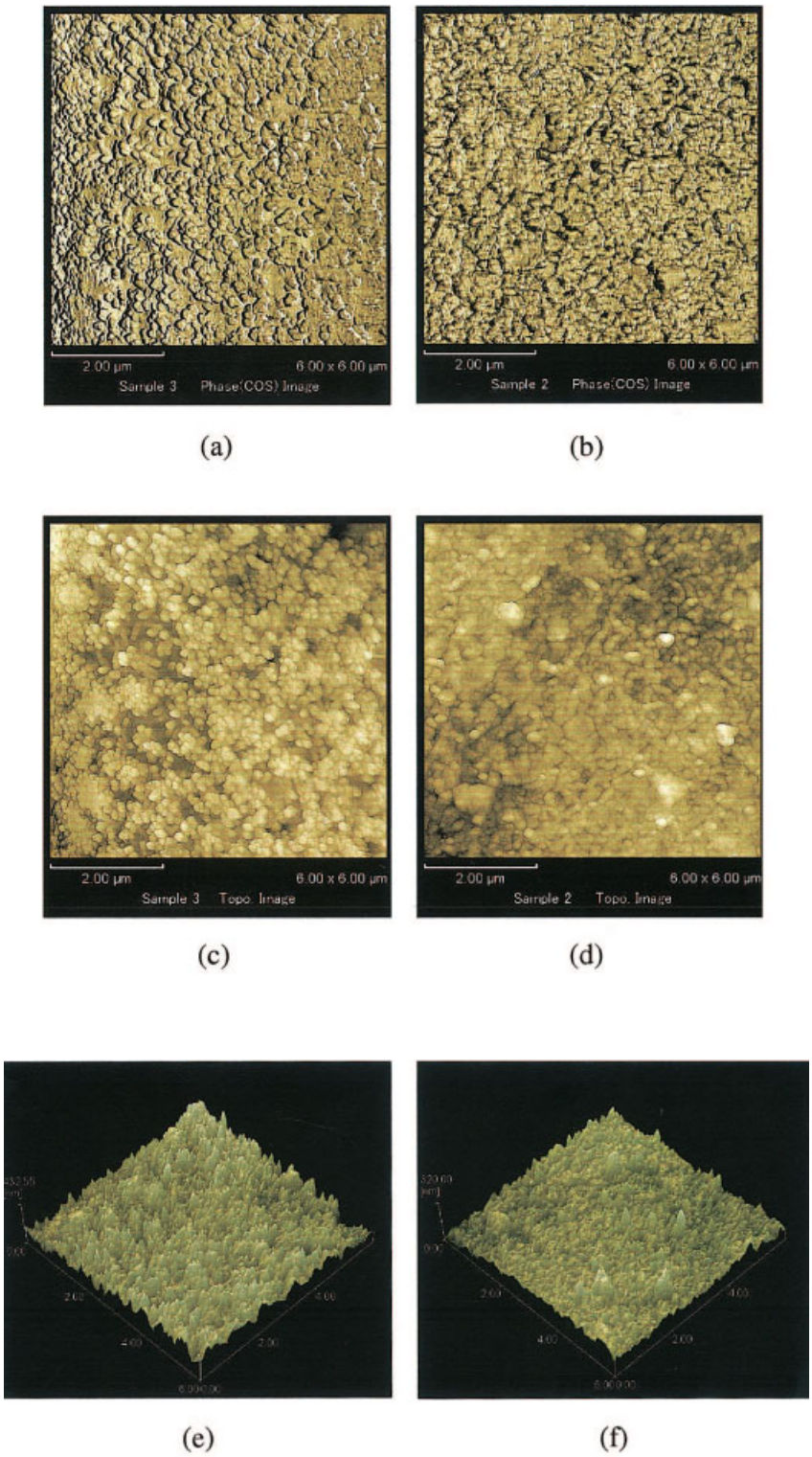

Figure 4 Morphology of the PPy coating layer. (a), (c), and (e) are on PPy-coated PA6 fiber; (b), (d), and (f) are on PPy-coated PU fiber. The scanned area is 6 × 6 μm. [Color figure can be viewed in the online issue, which is available at www.interscience.wiley.com.]

ciated with the force principally. Controlling the distance by varying the vertical position of the tip produces an image, which represents the topographic structure of the surface. However, in some case, deflection is not the most sensitive measurement, having a relatively small signal-to-noise ratio. Under tapping

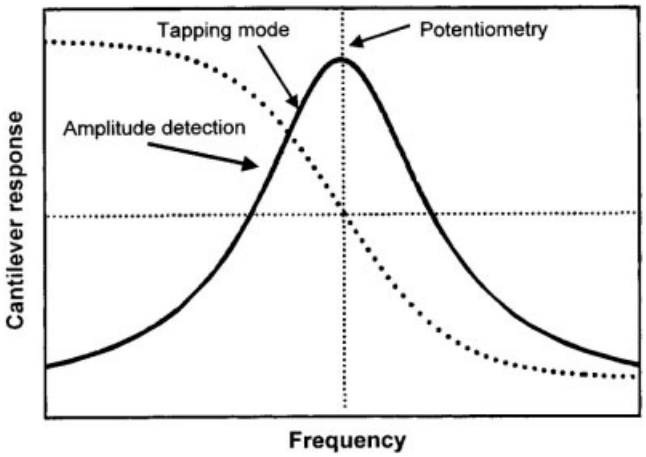

Figure 5 Frequency response of a typical AFM cantilever. The dashed line shows the phase of the cantilever osciallation.

mode, it is also possible to image based on the phase of the cantilever oscillation to improve signal-to-noise further. This is useful because any force gradient acting on the tip shifts the cantilever resonant frequency by decreasing the effective cantilever spring constant. This frequency shift is actually responsible for the change in amplitude. By measuring the change in phase as a function of sample position, high-resolution maps are obtained. The relationship between the frequency and response of a typical AFM cantilever is described in Figure 5.[18]

Going back to Figure 4, PPy particles appeared to have nucleated and then merged. For PA6 fiber base [(Fig. 4(a,c)], the PPy coating film is composed of well-connected PPy granules, covering up whole fiber surface with finer, denser, and more uniform grains than those of PPy on PU fiber base [Fig. 4(b,d)]. On the PU fiber base, the gap between the granules can be easily identified from the phase image. Figure 4(e) and f shows that the height of the rugged PPy coating layer on the PA6 fiber is much larger than that on the PU fiber.

Growth mode of PPy coating layer

A phenomenological film growth mode can help us to understand the difference in morphology and behavior. There are three basic models for describing the growth of a material deposited on a solid surface.[19,20] These models, although developed for atomic and ionic materials, may offer insight into polymer film growth by analogy. The three models are the island growth mode, the layer-by-layer growth mode, and the layer-plus-island growth mode. Of the three models, the third model seems to best fit the observation made in this study.

As shown in Figure 4, the PPy tended to form a connected layer on the substrate when polymerization was carried out. Before the well-connected first layer formed, PPy oligomer nucleated on the substrate in numerous places. For the PA6 fiber base, due to the strong interaction between the substrate and PPy, the nucleation rate is fast and the distance between nuclei is relatively small. The nuclei grows quickly in the lateral directions and spread throughout the surface of the fibers. The initially connected layer comes from multiple nucleation sites with either isotropic or anisotropic growth rates on the substrate. For the PU fiber base, the interaction between the substrate and PPy is relatively weak; therefore, the nucleation rate is slow and nuclei will grow both laterally and vertically as islands. Further work is required to investigate the interaction between the PPy and substrate polymers.

Electromechanical performance under tension

Electromechanical performance under simple tension

Before tests, the resistance was measured by the four-probe method with a Keithley 2010 Multimeter. It was noticed that, even under the same sample preparation conditions, the PPy-coated PA6 fibers possessed much higher conductivity than the PPy-coated PU fibers. The initial resistance of the PPy-coated PA6 fibers was

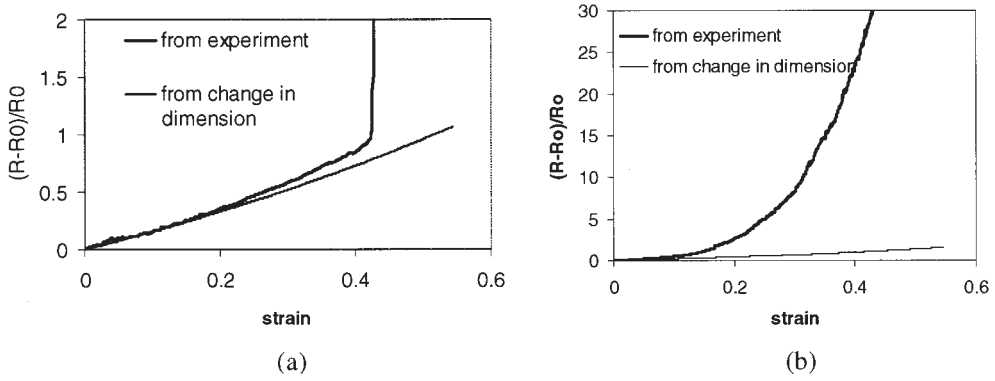

Figure 6 Typical $\Delta R/R_0$ vs. strain curves and the comparison of the results calculated from changing dimension of the specimen and measured from the experiments. (a) PPy-coated PA6 yarn; (b) PPy-coated PU yarn.

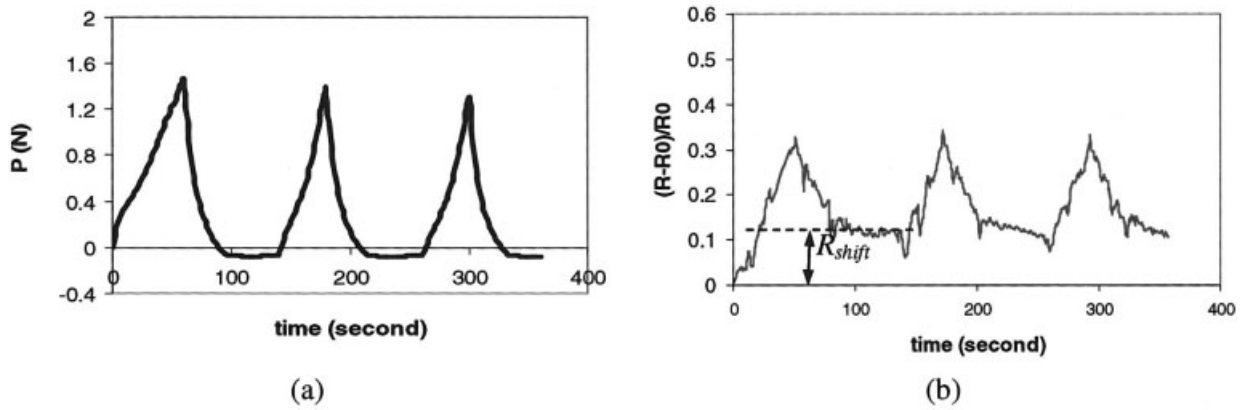

Figure 7 Variation in (a) applied load and (b) electric resistance during cyclic tension, unloading at a strain of 20% (PPy-coated PA6 yarn).

around 9 kΩ/cm, and yet for the PPy-coated PU fibers the initial resistance is almost 10 times higher.

By the electromechanical testing system, the relationship between the variation in electrical resistance and strain was obtained. Figure 6 depicts the typical curves of two kinds of samples. The electromechanical behavior of conductive composites strongly depends on the microstructure of the coating and the material of substrates. For the PPy-coated PA6 yarn, the variation in electrical resistance increased with increasing in the strain, and the relationship between $\Delta R/R_0$ and strain was nearly linear under tensile loading until the specimen fractured at a strain of 43%. However, for the PPy-coated PU yarn, within the strain of 10%, the values $\Delta R/R_0$ increased gradually, followed by a nonlinear and rapid increase. It was also noticed that the strain at which the resistance started to increase rapidly was much smaller than the ultimate strain of the PU fibers.

From our previous paper,[17,21] it was known that the variation in resistance from the change in dimension for PA6 fibers is slightly smaller than that from experimental values, but the two values are quite close to each other when the strain is less than 30%, as shown in Figure 6(a). Notably different for the PPy-coated PU fibers, the variation in the resistance from the change in dimension only contributes a small percentage of the total variation in resistance [Fig. 6(b)]. Therefore, the variation in $\Delta R/R_0$ is dominated by the change in its conductivity during tensile deformation, which will be further investigated.

Performance of conductive fibers under cyclic loading

A sensor may subject to repeated cyclic loading. Figure 7 shows typical plots of applied load versus time and normalized electrical resistance versus time for the PPy-coated PA6 fibers, obtained simultaneously during a cyclic tensile test. The specimens were unloaded at a strain of 20%, which is equal to 47% of the ultimate strain of the material. The applied load varied consistently as the number of cycle increased, except in the first cycle because the material behaved almost linearly after the strain of 15% (see Fig. 8). Examining the variation in electrical resistance, it was found that the resistance increased along with loading in the first cycle and decreased as unloading. However, at the end of the first cycle, the electrical resistance could not return to its initial value, R_0. This shift in resistance is attributed to the residual plastic deformation. The shift in electrical resistance is equal to

$$R_{shift} = \rho \frac{L_p}{A}, \tag{1}$$

where ρ is the linear resistivity and L_p is the length of the conductive specimen when load is reduced to zero. For the PPy-coated PA6 fiber, L_p was about 55.9 mm. This resistance remained unchanged until the fiber was extended again. Then, reloading caused the

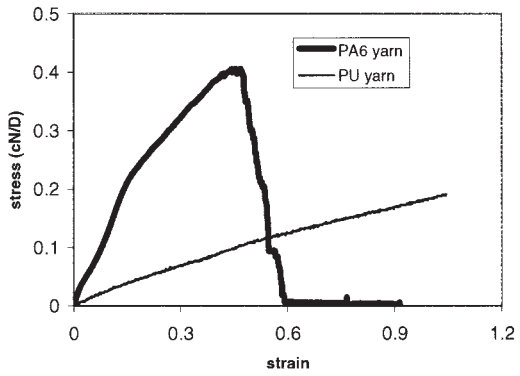

Figure 8 Stress vs. strain curves of bare PA6 yarn and PU yarn.

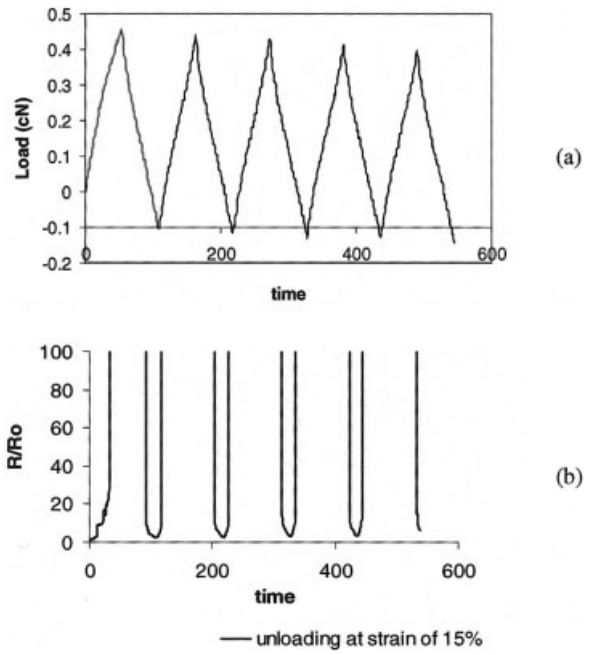

Figure 9 Variation in electric resistance of PPy-coated PU yarn during cyclic tension, unloading at a strain level of 15%. (a) Load vs. time curve; (b) electrical resistance vs. time curve.

electrical resistance to increase, and in subsequent unloading the electrical resistance varied in a manner similar to that during the first unloading. As cyclic tension progressed, the electrical resistance varied along with the applied load correspondingly.

The PPy-coated PU yarn behaved differently under cyclic tension. Figure 9 gives the response of PPy-coated PU yarn under repeated tension with unloading at a strain level of 15%. The applied load varied cyclically with time; however, the electrical resistance changed differently from what we measured for the PPy-coated PA6 yarn. In the first cycle, the electrical resistance increased until it overflowed in loading and returned to its original value from a state of overflow in unloading. In the following cycles, the electrical resistance varied in the same way as it did in the first cycle.

A sensing material should possess characteristics such as linearity, repeatability, and sensitivity. From the above investigation, it is known that PPy-coated PA6 fibers can provide much better sensing performance than PPy-coated PU fibers.

Investigation on mechanisms

The SEM microphotographs of two kinds of fibers at different strain levels are shown in Figures 10 and 11 with magnification of 5 and 2 k, respectively. The mechanisms governing the behavior of the two kinds of conductive fibers are different from each other.

After polymerization of pyrrole, the PPy encased each single fiber of the yarn with a smooth, coherent layer of electrically conductive polymer, whereas on the surface of PU fibers, microstriations along circumferential direction were found even before the specimen was extended ($\varepsilon_e = 0$). This phenomenon can be explained by the morphology of PPy coating layers and the mechanical properties of the substrates. SPM observation revealed that the PPy coating on PU fibers is not as fine, dense, and uniform as that on PA6 fibers. The gap between the granules can be easily identified. On the other hand, PPy has a modulus of GPa while PU has that of MPa. The hard coating on the soft and extensible fiber is very easily damaged. Thus, even a slight extension during specimen preparation may cause these microdefects on the surface.

The different electromechanical behaviors of two kinds of samples were described above. From the *in situ* SEM observations, it is known that the coating layer of the PA6 fibers can remain complete without apparent damage until the longitudinal strain reaches about 25%. Once damage occurred on the surface of the fiber, it fractured abruptly. The resistance variation mainly resulted from the change in dimension of the fibers. The discrepancy between the resistance variation from the dimensional change and the measured result is attributed to the damage on the coating layer and breakage of the individual fibers.

In contrast, for the PPy-coated PU fibers, the transverse cracks become wider and longer with increasing tensile deformation. However, below the longitudinal strain of 15–25%, a conducting PPy network still exists, which forms the current conducting paths, so that the PPy-coated PU fibers still possess current-carrying capacity. The resistance variation with the applied strain mainly attributes to these microcracks occurring on the coating layer. With the accumulation of the damage, the continuous current conductive paths become longer and thinner and the electrical resistance increases rapidly until the accumulated damage of the coating layer reaches a level sufficient to block electrical conductivity of the PPy-coated fibers. The microcracks that occurred on the surface of the conductive fibers are similar to what may happen in some thin, layered devices in electronics, such as liquid crystal displays, organic solar cells, and organic light-emitting display. In these cases, thin brittle material, such as indium-tin oxide, was deposited on polymeric substrate and may fracture under tension.

Under cyclic tension, the electrical resistance of PPy-coated PU fibers increased, followed by a decrease in the first cycle, which can be interpreted as the transverse cracks opening and closing. In the following cycle, the cracks reopened and reclosed at loading and unloading, respectively, causing the electrical resistance to vary abruptly, not gradually, as shown in Figure 9.

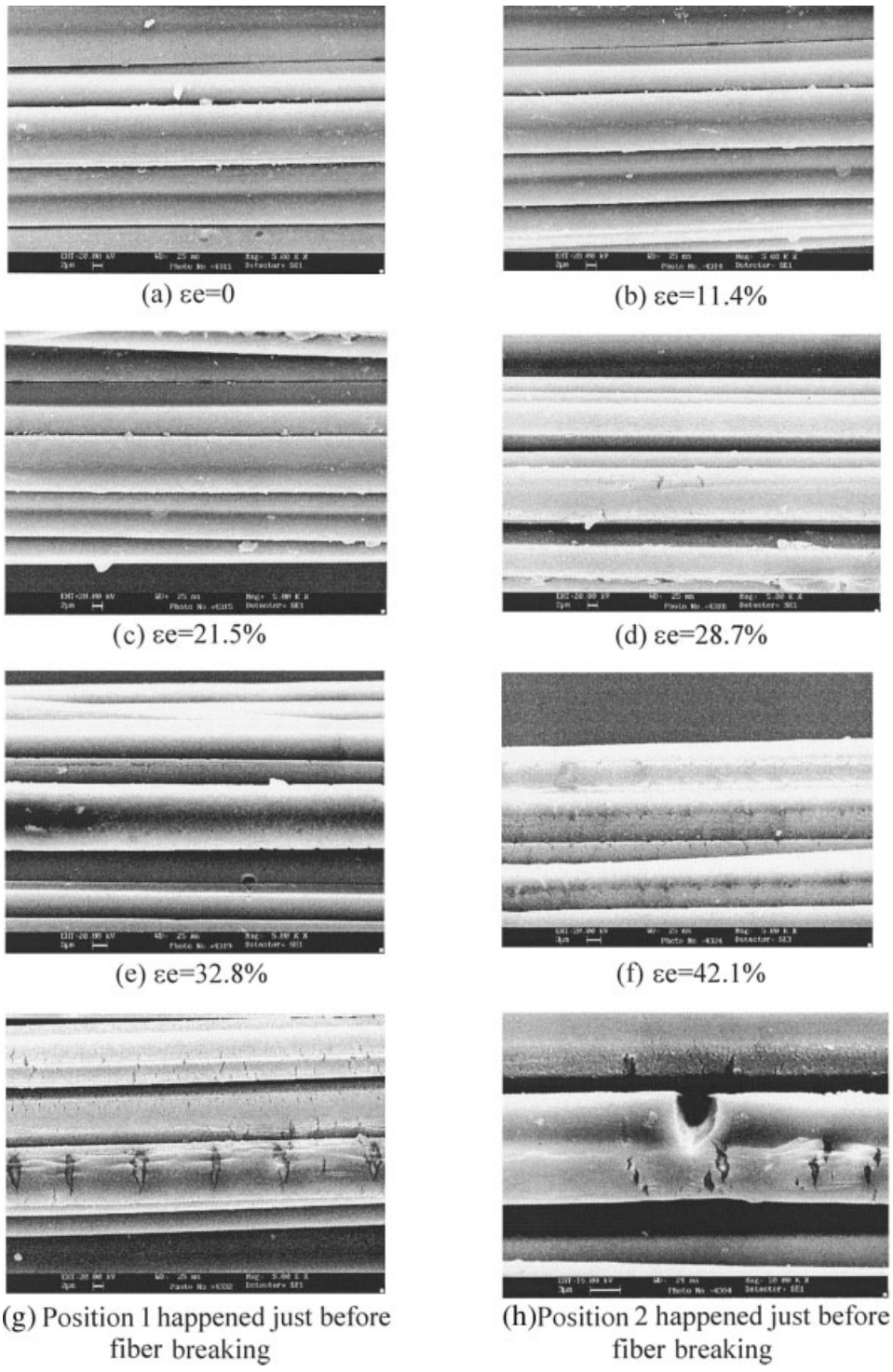

Figure 10 SEM microphotographs of PPy-coated PA6 yarn at different strain level.

This different behavior of two kinds of conductive fibers can be further explained by the difference in mechanical properties. Figure 8 shows that PU yarn has much larger ultimate strain compared with PA6 yarn. The former is 560% and the latter is only about 46%. Young's moduli of the PA6 and PU yarns are about 1.37 and 0.25 cN/D, respectively. The former is about 5.5 times that of the latter. The large difference in Young's moduli can interpret why the transverse cracks occur on the surface of the PPy-coated PU fibers.

In fact, under the same level of the applied stress, the PPy-coated PU yarn will experience much larger deformation than the PPy-coated PA6 yarn. A larger strain must result in higher strain energy. It is the

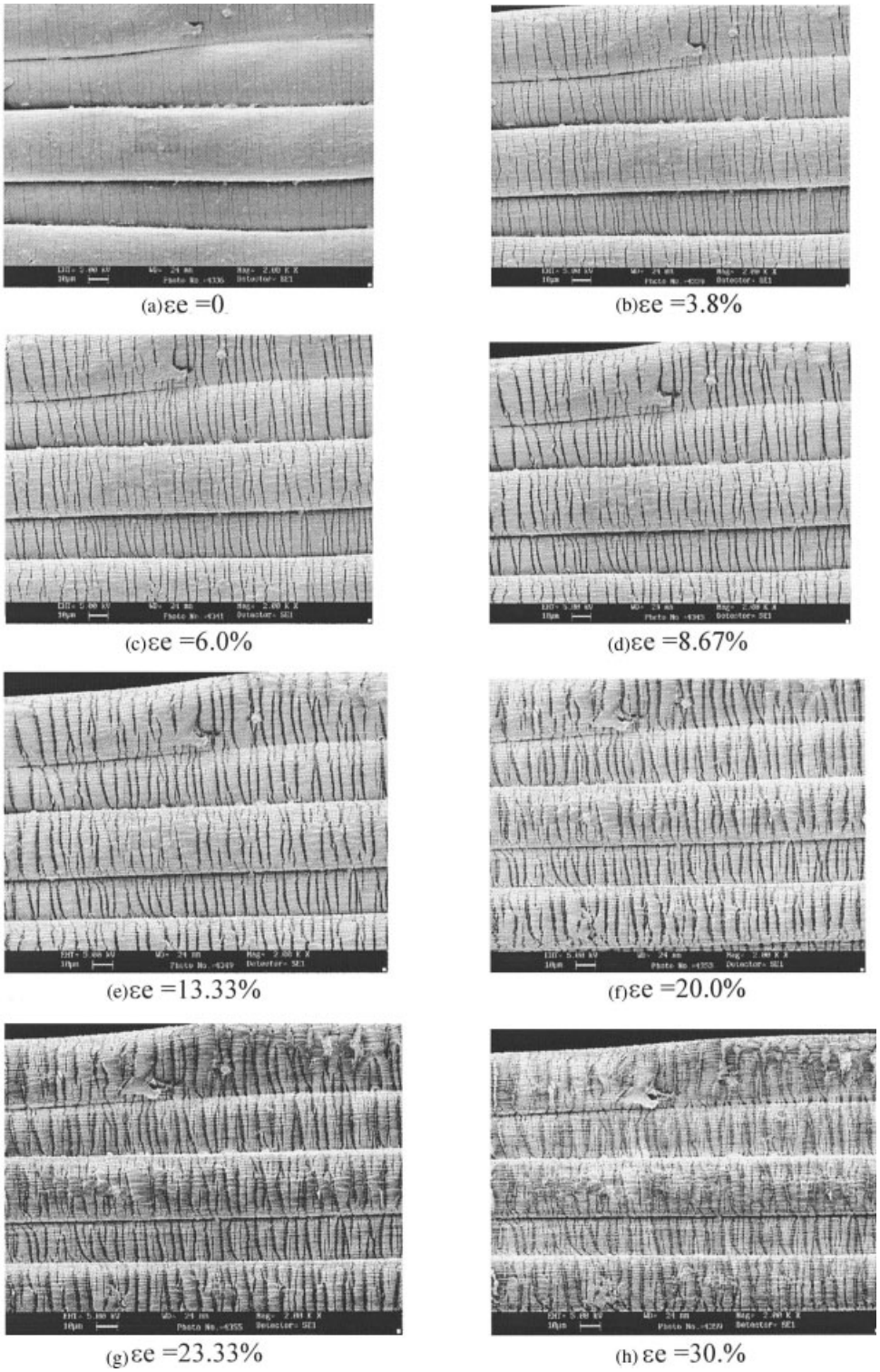

Figure 11 SEM microphotographs of PPy-coated PU yarn at different strain level.

surface cracks that release the large strain energy stored in the PPy-coated PU yarn. The steady-state energy release rate, G_c, is given as[22,23]

$$G_c = \frac{1}{2} E_f \epsilon^2 \pi h_f g(\alpha,\beta). \quad (2)$$

The factor g (α, β) is a function of the Dundurs parameters, α and β, which for plane strain condition are given by

$$\alpha = \frac{E_f - E_s}{E_f + E_s} \quad \beta = \frac{G_f(1-2v_s) - G_s(1-2v_f)}{2G_f(1-v_s) + 2G_s(1-v_f)}, \quad (3)$$

where E is the plane strain tensile modulus and G is the shear modulus. The subscripts, f and s, stand for the coating film and substrate, respectively. Of these two parameters, α is much more important. Restricting β to the practical limits of $\beta = 0$ or $\beta = \alpha/4$, the function, g, will increase with parameter α. Therefore, the larger difference between Young's moduli of the coating film and the substrate will lead to easy cracking.

CONCLUSIONS

This study investigates the relationship between the morphology and electromechanical behavior of the electrically conductive fibers and analyzes the mechanisms governing their electromechanical behavior based on microscale observations by means of SPM, AFM with current measurement, and SEM. The following can be concluded:

(1) The electromechanical behavior of the conductive composites depends strongly on the microstructure of the coating layer and the material of the substrate. On PA6 base, PPy forms a continuous layer with finer, denser, and more uniform grains than those on the PU base. A smooth and uniform coating and matched mechanical properties will lead to a satisfied performance of conductive fiber sensors. The relationship between the fractional increment in resistance, $\Delta R/R_0$, and the applied strain is reasonably linear, which is of practical importance in sensing applications.

(2) The variation in resistance for the PPy-coated PA6 fibers results from the change in the dimension of the fibers. By contrast, the variation in resistance with the applied strain for PPy-coated PU fibers is mainly attributed to the damage on the coating layer.

We thank Seiko Instruments and Comfort Technology (Asia) for technical assistance in SPM measurements. We also wish to acknowledge the Innovation and Technology Commission of the Hong Kong SAR government for the partial support under ITF project: ITS/11/02 and the Hong Kong Research Grants Council under grant: poly 5160/02E.

References

1. Tao, X. M. Smart Fibers, Fabrics and Clothing, The Textile Institute: England, 2001.
2. Cho, J. W.; Choi, J. S. J Appl Polym Sci 2000, 2082, 77.
3. Wang, X.; Chung, D. D. L. Smart Mater Struct 1996, 5, 796.
4. Cho, J. W.; Choi, J. S.; Yoon, Y. S. J Appl Polym Sci 2002, 83, 2447.
5. Fankhanel, B.; Muller, E.; Mosler, U.; Siegel, W.; Beier, W. Compos Sci Technol 2001, 61, 825.
6. Schulte, K.; Baron, C.; Compos Sci Technol 1989, 36, 63.
7. Wallance, G. G.; Spinks, M. G.; Kane-Maguire, L.A.P.; Teasdale, P. R. Conductive Electroactive Polymers; CRC Press: New York, 2003.
8. Thiéblemont, J. C.; Brun, A.; Marty, J.; Planche, M. F.; Calo, P. Polymer 1995, 36, 1605.
9. Omastova, M.; Pavlinec, J.; Pionteck, J; Simon, F. Polym Int 1997, 43, 109.
10. Ruckenstein, E.; Chen, J. H. Polymer 1991, 32, 1230.
11. Truong, V.-T.; Riddell, S. Z.; Muscat, R. F. J. Mater Sci 1998, 33, 4971.
12. Chen, X. B.; Devaux, J.; Issi, J.-P.; Billaud, D. Polym Eng Sci 1995, 35, 637.
13. Pionteck, J; Omastova, M.; Poetschke, P.; Simon, F.; Chodak, I. J. Macromolr Sci Phys 1999, B38, 737.
14. Chen, Y. P.; Qian, R. Y.; Li, G.; Li, Y. Polym Commun 1991, 32, 189.
15. De Rossi, D.; Mazzoldi, A.; Carpi, F.; Scilingo, E. P.; Lorussi, F.; Tognetti, A. In Proceedings of IEEE Sensors, 2002, 1, 1608.
16. Kim, M. S.; Kim, H. K.; Byun, S. W.; Jeong, S. H.; Hong, Y. K.; Jood, J. S.; Song, K. T.; Kim, J. K.; Lee, C. J.; Lee, J. Y. Synth Metals 2002, 126, 233.
17. Xue, P.; Tao, X. M.; Yu, T. X.; Kwok, Keith W. Y.; Leung, M. Y. Textile Res J 2004, 74, 929.
18. Dawn, B. Scanning Probe Microscopy and Spectroscopy-Theory, Techniques, and Applications, 2nd ed.; Wiley: New York, 2001.
19. Stokes, R. J.; Evans, D. F. Fundamentals of Interfacial Engineering, Wiley-VCH: New York, 1997.
20. Yuan, W. L.; O'Rear, E. A.; Cho, G.; Funkhouser, G. P.; Glatzhofer, D. T. Thin Solid Films 2001, 385, 96.
21. Xue, P.; Tao, X. M. In Wearable Electronics and Photonics; Tao, X.M., Ed.; Woodhead: UK, 2005, Chapter 5.
22. Beuth, J. J. Int J Solid Struct 1992 29, 1657.
23. Chen, Z.; Cottrell, B.; Wong, W. Eng Fracture Mech 2002, 69, 597.